Understanding and Improving Mechanical Stability in Electrodeposited Cu and Bi for Dynamic Windows Based on Reversible Metal Electrodeposition

Gabriel R. McAndrews, Andrew L. Yeang, Yuchun Cai, Christopher J. Barile, and Michael D. McGehee

Dynamic windows based on reversible metal electrodeposition (RME) can electronically adjust light transmission from ≈70% to <0.1% to improve building aesthetics and energy efficiency by controlling light and heat flow. For RME devices using Cu and Bi, the windows reach "privacy state" (<0.1% transmission) when ≈180 nm of metal is electrodeposited on the transparent conducting electrode. When films with a plated atomic Cu–Bi ratio of ≈2:1 rest in the privacy state, sinusoidal cracks form across the entire film, and the metal delaminates in <1 day. This mechanical failure renders the window unusable as specks of metal are visually unattractive and reduce the dynamic range of the window. The Cu–Bi film is stress free upon deposition, but after 4 h of resting, 38 MPa of tensile stress develops. The tension in Cu–Bi and Cu films combined with the $Cu(ClO_4)_2$ in the electrolyte results in severe, widespread fractures and delamination due to stress corrosion cracking. In contrast, electrodeposited Bi films have compressive stress, likely due to high self-diffusion and insertion of atoms into grain boundaries while plating, which results in a Bi-based dynamic window with crack-free resting stability that exceeds 9 weeks.

1. Introduction

Reversible metal electrodeposition (RME) is a growing field with many applications ranging from batteries (e.g., Li, Na, and Zn) to dynamic glazings with applications for thermal emissivity (e.g., Ag) or windows (e.g., Cu, Bi, Ag, and Zn). In each of these systems, a layer of metal is electroplated for the system's designed purpose: energy storage for batteries,[1–4] infrared light modulation for dynamic thermal emissivity,[5] and visible light modulation for dynamic windows.[6–8] The mechanical stability of the electrodeposited films is paramount for the devices' durability in practical applications. Mechanical failure can occur in the form of detached dendrites, "dead" metal, pits, and cracked or delaminated films, which usually result in loss of active material leading to device failure. The mechanics of electrodeposited Li has been extensively studied for Li metal batteries.[9,10]

Dynamic windows allow for electronic and user control over light and heat flow into and out of buildings. They can improve building efficiency up to 20% due to reduced lighting, heating, and cooling loads while also allowing people to reduce glare while maintaining clear views.[11] Their implementation can improve worker productivity by 2% due to reduction in headaches and eyestrain.[12,13] RME dynamic windows are an exciting area of research because they have the potential to overcome the limitations of current (ion-intercalation based) dynamic windows with respect to cost, color, and dynamic range.[14–21] These RME dynamic windows operate by reducing metal ions (e.g., Cu^{2+}, Bi^{3+}, Zn^{2+}, and Ag^+) to their metallic form from a nearly colorless electrolyte onto a transparent conducting oxide (TCO). While a reductive potential is held, the metal film nucleates and grows on the TCO working electrode, decreasing the film's transmission. When the polarity of the potential is switched, the metal atoms oxidize and return in their cationic form to the electrolyte, restoring the transparency of the window. A metal mesh is used as a transparent counter electrode to balance the redox reactions on the TCO (by oxidizing metal for window tinting and reducing metal ions for window bleaching).

One unique advantage to using RME for light modulation is the ability to tune the transmission state well below 1% transparency. We have recently shown that the use of a small amount of polymer inhibitor (0.1 w/v%) enables RME dynamic windows to reach extremely low transmission states

G. R. McAndrews, M. D. McGehee
Materials Science and Engineering Program
University of Colorado Boulder
Boulder, CO 80303, USA
E-mail: michael.mcgehee@colorado.edu
A. L. Yeang, M. D. McGehee
Department of Chemical and Biological Engineering
University of Colorado Boulder
Boulder, CO 80303, USA
Y. Cai
Department of Chemistry
University of Colorado Boulder
Boulder, CO 80303, USA
C. J. Barile
Department of Chemistry
University of Nevada Reno
Reno, NV 89503, USA

**ADVANCED
SCIENCE NEWS**
www.advancedsciencenews.com

**ADVANCED
ENERGY
MATERIALS**
www.advenergymat.de

(<0.01%) with superb color neutrality (C* < 10) at large scale (30 cm × 30 cm) because the film that is deposited is uniform, smooth, and compact.[19] We also discussed the design principles of the metal mesh counter electrode to enable durable privacy cycling.[22] In this manuscript, we focus on the mechanical reliability of these electroplated metal films. We show that windows made using the same Cu–Bi perchlorate electrolyte described in our recent publications[19,22] have a mechanical resting stability problem, whereby the Cu–Bi metal films crack and delaminate after 12 h of resting. We perform stress measurements and take microscope images for films of different metals (Cu–Bi, Cu, and Bi). The original co-deposition using Cu and Bi in an atomic plated ratio of ≈2:1 to 3:1 shows an increase in tensile stress while resting in the electrolyte due to impurity desorption. The failure mode in these films is consistent with stress corrosion cracking (SCC), which occurs in films of susceptible materials under tension in a corrosive environment. Without proper mitigation, SCC has resulted in catastrophic failure such as the collapse of the Silver Bridge in 1967.[23] Due to the safety implications the field of SCC has attracted considerable attention for a variety of materials including stainless steel used in vessels or pipework[24] as well as thin film coatings of brass or copper used in the storage of nuclear waste.[25,26] In this work we demonstrate a metal film (Bi) with enhanced mechanical stability due to its ductility, intrinsic resistance to SCC, and compressive stress. Finally, we construct a Bi-based device and show a >126× improvement in mechanical stability of the Bi film, demonstrating no mechanical failure over >2 months at rest in five 5 cm × 5 cm devices.

2. Results and Discussion

2.1. Mechanical Failure in Electrodeposited Cu–Bi Systems

Electroplated Cu–Bi films have been used in RME windows with impressive performance metrics regarding color, switching speed, dynamic range, and scale.[14–19] Thus, it is imperative that these films exhibit superb mechanical durability for practical purposes as a cracked film is ineffective at blocking light and delaminated films leave metal flakes that are electrochemically unusable and visually unappealing. **Figure 1** displays microscope images of our standard device resting on the benchtop after being tinted to privacy state transmission (0.1% transmission). While there is no mechanical failure at the initial tinting or after 4 h resting (Figure 1a,b), there is clear evidence of sinusoidal and spiral fractures after 12 h followed by severe delamination (Figure 1c,d and Figure S1, Supporting Information).[27–29] We refer to the complex failure pattern as "puzzle piece fracture," which can be explained by in-plane equibiaxial stress and the attractive tendency of propagating cracks (Figure S2, Supporting Information).[27,30] The fractured and delaminated pieces of the film cover almost the entire film, are obvious by eye, and result in the loss of active material for use in future plating and in a window which ineffectively blocks light.

2.1.1. Stress Measurements

To identify the stress present in Cu–Bi films we conducted substrate curvature measurements. The deflection was measured
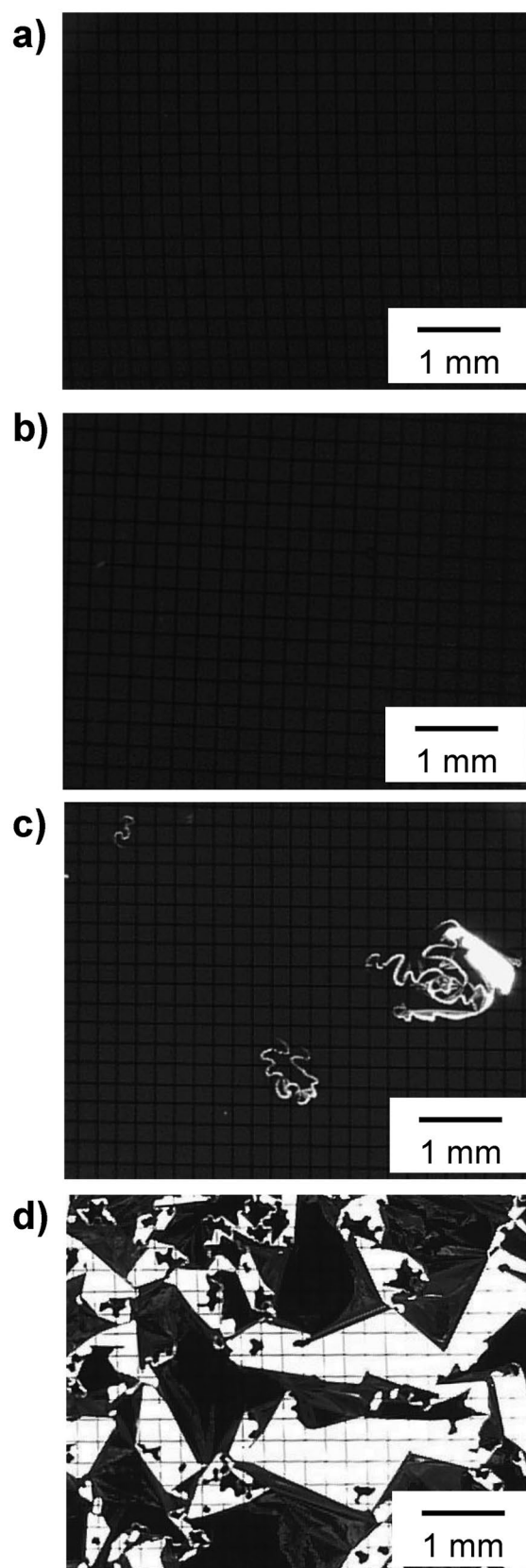

Figure 1. Microscope images of Cu–Bi device tinted to privacy state transmission at a) 0, b) 4, c) 12, and c) 24 h after tinting and unplugging.
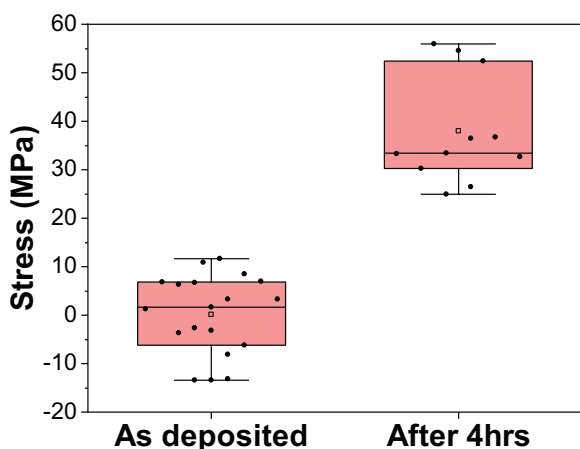
2202843 (2 of 8)

Figure 2. Stress in electrodeposited Cu–Bi films immediately after deposition and after 4 h of soaking in its electrolyte calculated with substrate curvature measurements. Each data point corresponds to a unique scan.

at four lines for each thin-glass substrate with a Dektak profilometer before deposition, immediately after deposition, and after the Cu–Bi films soaked in its plating electrolyte in an oxygen-free environment for 4 h (Figure S3 and Note S1, Supporting Information). Each scan was fit using a locally weighted least square regression to determine the curvature as detailed by Volinsky et al. (Figures S5 and S6; Note S2, Supporting Information).[31] The Stoney equation (Equation (1)) was applied to determine the in-plane biaxial stress:[32]

$$\sigma_f = \left(\frac{E_s}{1 - \nu_s} \right) \frac{t_s^2}{6 t_f} \Delta\kappa \tag{1}$$

Where E_s is the substrate Young's modulus, ν_s is the substrate Poisson ratio, t_s is the substrate thickness, t_f is the Cu–Bi film thickness, and $\Delta\kappa$ is the substrate curvature change. The Cu–Bi film thickness at various transmission states was measured using Dektak profilometry (Figure S7, Supporting Information). The residual stress in the as deposited Cu–Bi plated to privacy was near zero (0.2 ± 7.9 MPa), but after 4 h of soaking in its electrolyte the stress increased into tension (37.9 ± 10.6 MPa) (**Figure 2**). Several mechanisms can be used to explain the initial and transient stresses observed in electrodeposited Cu–Bi films.

2.1.2. Sources of Stress

During the co-deposition of the Cu–Bi films, isolated grains coalesce with neighboring grains to minimize surface energy and to contribute tensile stress (**Figure 3**a). Coalescence has been established as a primary source of tensile stress for electrodeposited metals such as Cu, and the magnitude of stress is dependent on the rate of deposition and corresponding grain size.[33,34] The contribution of tensile stress from coalescence for Cu–Bi films likely occurs prior to the privacy transmission ($t_f \approx 180$ nm) due to its deposition resemblance to Volmer–Webber type growth.[35,36] SEM images in this work and previous publications indicate that grains begin to impinge upon
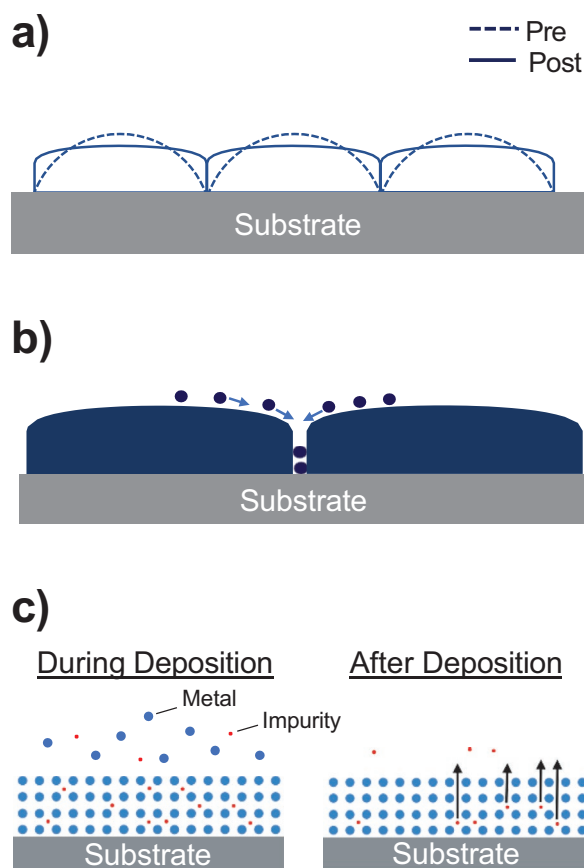

Figure 3. Schematics for mechanisms that induce either tensile or compressive stress. a) Crystallite coalescence and the formation of grain boundaries (tensile stress). Adapted with permission.[44] Copyright 2000, IOP Publishing. b) Adatom insertion into grain boundary (compression). Adapted with permission.[33] Copyright 2013, IOP Publishing. c) Impurity desorption after electrodeposition (blue-metal; red-impurity) (compression during plating that lessens after desorption). Adapted with permission.[38] Copyright 1992, IOP Publishing.

each other at privacy transmission and partial coalescence occurs (Figure S8, Supporting Information).[19]

During coalescence, there is the potential for adatom insertion into the grain boundaries, which will result in a lower residual stress for electrodeposited metals. A chemical potential difference between atoms on the surface and in the grain boundary provides a driving force for excess atoms to be inserted into the grain boundary (Figure 3b). Therefore, the rate of grain boundary coalescence (tensile stress) and adatom insertion (compressive stress) determines the resulting residual stress at the privacy state. For example, Hearne et al. demonstrated that electrodeposited Ni films at fast deposition rates have tensile stress as there is minimal opportunity for excess atoms to insert into the grain boundary prior to the growth of the grain boundary.[37] On the other hand, compressive stress was obtained due to appreciable adatom insertion at slow deposition rates.

Impurity incorporation into the Cu–Bi film during deposition should contribute compressive stress, and if these impurities desorb after plating the compressive contribution would be lessened (Figure 3c).[38] Ziebell and Schuh observed a 30 ± 15 MPa increase in tensile stress for electrodeposited Ni–W

**ADVANCED
SCIENCE NEWS**

www.advancedsciencenews.com

**ADVANCED
ENERGY
MATERIALS**

www.advenergymat.de

films after degassing co-deposited hydrogen under vacuum.[39] For electrodeposited Cu, hydrogen, oxygen, and organic impurities have been shown to induce compression up to the GPa order.[38,40,41] Armyanov and Sotirova developed a relationship between the concentration of desorbed interstitial impurities such as hydrogen and the corresponding stress (Equation (2)):

$$C_H(t) = \frac{3}{\Delta\Omega/\Omega} \frac{\Delta\sigma_f(t)}{M_f} \tag{2}$$

Where $C_H(t)$ is the concentration of hydrogen that diffuses in or out of the film, Ω is the atomic volume of the film material, $\Delta\Omega$ is the change in atomic volume with hydrogen, M_f is the reduced elastic modulus, and $\Delta\sigma_f(t)$ is the change in stress due to absorption or desorption.[37,42] The observed increase in tensile stress of 38 MPa in the Cu–Bi system after 4 h would correspond to ≈0.6 at% hydrogen desorption. We used an electrochemical quartz crystal microbalance (eQCM) and calculated the metal plating charge efficiency to be ≈93%, which suggests side reactions and impurity co-deposition are possible (See Note S3, Supporting Information). Furthermore, the presence of blisters in Cu–Bi suggests that hydrogen or oxygen is incorporated into the film during electrodeposition (Figure S10, Supporting Information) and released later. Absorbed atomic hydrogen tends to migrate to voids and accumulation results in H_2 gas formation and pressure build-up followed by blister formation.[43] Dissolved oxygen may also act as an impurity with the potential for blister formation. Therefore, it is reasonable to assume that the increase in tensile stress for electrodeposited Cu–Bi after 4 h originates from a minimal quantity of impurity desorption.

Alternative explanations for the transient stress behavior such as grain growth, further coalescence, and galvanic displacement are less probable. Self-annealing of electrodeposited Cu at room temperature has been reported to introduce tensile stress through the elimination of excess volume at grain boundaries.[41] However, there is no substantial evidence of grain growth for Cu–Bi films even after 8 h (Figure S11, Supporting Information). In addition, the strongest contribution from coalescence for electrodeposited metals typically occurs before hundreds of nanometers are plated.[35,44] Galvanic displacement of Bi by Cu has the potential to introduce stress similar to a Kirkendall-type exchange, which has been shown to introduce tensile stress.[45] Despite the thermodynamic driving force for galvanic displacement, we show in Note S4, Supporting Information, that galvanic displacement (driving force of –7.6 kJ mol⁻¹) is not the primary cause of the observed fractures and delamination.

2.2. Single Metal Systems

We explored single metal systems with Cu or Bi as the active metals to avoid any potential influence of galvanic displacement on the resulting fractures and delamination. Prior to testing the resting stability, the as-deposited biaxial strain in electrodeposited Cu and Bi single metals was determined with X-ray diffraction (XRD):Sin²ψ measurements, and the stress was inferred (Figure S13, Supporting Information).[46,47] This method is routinely used to assess residual stress in polycrystalline metal films[46,48,49] and details can be found in Note S5, Supporting
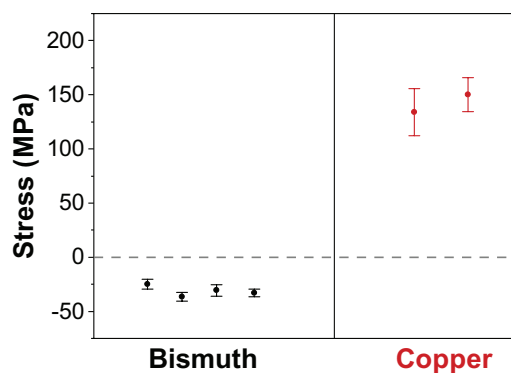

Figure 4. Residual stress in electrodeposited single metals bismuth (black) and copper (red) determined from XRD: Sin²ψ measurements. Each data point represents the stress for an individual electrodeposited film.

Information. In short, in-plane biaxial strain results in dissimilar lattice spacings between planes parallel and perpendicular to the substrate which can be probed by tilting the thin film through the angle ψ. Interestingly, Cu deposited under residual tension (142.1 ± 26.9 MPa) while Bi deposited with compression (–31.2 ± 8.8 MPa) (**Figure 4**). When these films soak in their as-deposited electrolytes, the electrodeposited Cu films exhibit widespread sinusoidal fractures and delaminate within 24 h, similar to the mechanical failure observed in Cu–Bi. On the other hand, the electrodeposited Bi films were stable for >7 days (Table S3, Supporting Information).

2.2.1. Cu-Containing Systems Mechanically Degrade due to SCC

The residual tensile stress observed for electrodeposited Cu can best be understood with the crystallite coalescence model. Chason et al. developed a rate dependent stress for electrodeposited Cu and hypothesized that at fast plating rates crystallite coalesce occurs, rather than adatom insertion, which results in tensile stress.[33,50] AFM images of Cu films plated to privacy state transmission show clusters of grains impinging on each other which provides evidence of grain coalescence (Figure S14, Supporting Information). At the fast deposition rates necessary for reasonable window tinting speeds, tensile stress is expected. However, it is not obvious that fracture and delamination would occur since Cu is a relatively ductile metal, at least in noncorrosive environments.[51]

The mechanical failure of electrodeposited Cu and Cu–Bi can be interpreted in the context of SCC.[25] The electrolyte environment can induce film rupture, propagation, and eventual delamination even at stress values below the yield stress of the metal. SCC requires three components: a susceptible material, tensile stress, and a corrosive environment.[52] At room temperature, Cu has been shown to be intrinsically susceptible to SCC due to its low self-diffusion coefficient and inability to relieve tensile stress with dislocation movement.[53–55] We have established the presence of tensile stress in the electrodeposited Cu (Figure 4). We will show that the presence of $Cu(ClO_4)_2$ in our acidic electrolyte contributes to the corrosive environment, the final component of SCC.[54,56]

ADVANCED
SCIENCE NEWS

www.advancedsciencenews.com

ADVANCED
ENERGY
MATERIALS

www.advenergymat.de

For Cu films, we observed a strong dependence of the fracture propagation rate on the concentration of Cu^{2+} in the electrolyte ($Cu(ClO_4)_2$) (Table S4, Supporting Information). With 5 and 10 mm $[Cu^{2+}]$ through thickness cracks propagated >2 cm in less than 1 day (Figure S15, Supporting Information), but with 0.5 mm $[Cu^{2+}]$ there were no signs of fractures until 14 days of electrolyte soaking. These findings echo those of Galvele and colleagues that show $[Cu^{2+}]$ corresponded to the rate of SCC for electrodeposited brass.[54] Galvele proposed a surface mobility mechanism to explain the relationship between $[Cu^{2+}]$ and crack propagation rates. He theorized that certain components of the electrolyte increase the surface mobility and result in the net motion of atoms out of crack tips and therefore the propagation of the crack.[53] The exchange current density for Cu reduction and oxidation ($Cu^0 = Cu^{2+}+2e^-$) acts as a straightforward quantity to measure that directly correlates to surface diffusivity and the crack propagation rate as it quantifies how much current is flowing in equilibrium. Indeed, for electrodeposited Cu the equilibrium ion exchange current is dependent on the $[Cu^{2+}]$ (Figure S16 and Table S4, Supporting Information). The exchange current density is likely to be high for Cu^{2+} containing electrolytes due to the relative stability of Cu^+, which is an intermediate in metal deposition according to Marcus theory, compared to other metal intermediates (e.g., Zn^+, Bi^{2+}, and Bi^+).[57]

The severe fractures observed in the Cu–Bi dynamic windows are likely a result of SCC (Figure 1). Specifically, the presence of elevated $[Cu^{2+}]$ in the electrolyte promotes rapid ion exchange and crack propagation at low stress (37.9 ± 10.6 MPa) (Figure 2 and Table S4, Supporting Information). Unfortunately, despite the amorphous nature of the Cu–Bi (see XRD data in Figure S11, Supporting Information) the metal did not experience the benefits of amorphous metals such as wear and corrosion resistance and increased strength compared to their crystalline counterparts.[58] In fact, small amounts of Bi segregated at Cu grain boundaries can embrittle Cu–Bi systems.[59,60]

The Cu–Bi and Cu films delaminated from the indium tin oxide (ITO) following their fracture due to a loss of adhesion at the interface with the Pt-ITO surface. For Cu, water exposure (pH = 7) has been shown to induce a 90% decrease in interfacial toughness compared with air exposure.[61] The loss of adhesion is presumably intensified in the corrosive perchloric acid environment and the fractures allow for increased area for the loss of adhesion and tensile stress to promote delamination. We discuss the factors affecting the adhesion of our Cu–Bi film to Pt-ITO in Note S6, Supporting Information.

A metal electrodeposited under compressive stress that does not have intrinsic susceptibility to SCC offers the best solution to enhance the resting stability for dynamic window application. It is important to note that extreme compression can result in buckles, blisters, and delamination, so a slightly compressive stress is ideal.[62,63]

2.2.2. Bi Only Systems Deposit under Compression and Demonstrate Superior Mechanical Stability

Bi-based dynamic windows should be resistant to SCC because it lacks two of its three requirements. First, Bi electrodeposits under compression (−31.2 ± 8.8 MPa) probably due to adatom insertion into grain boundaries driven by high self-diffusion.[64,65] Further, Bi is not intrinsically susceptible to SCC due to its low melting temperature and high self-diffusion coefficient. In this case, stress relief can occur with dislocation movement rather than crack propagation.[53]

Thus, we tested the mechanical stability of the Bi-based system. We tinted 5 cm × 5 cm Bi-based windows to privacy state transmission with comparable performance metrics to devices described in previous work (Figure S19, Supporting Information).[19] No evidence of fractures or other signs of mechanical failure was observed by visual inspection with a confocal microscope after the deposited Bi rested for longer than 9 weeks. The mechanical stability of the Bi-based windows was consistent and repeatable as five devices were crack-free as shown in representative microscope images (**Figure 5** and Note S7, Supporting Information). In addition, we show there is no increase in transmission over this time, further demonstrating the superior resting stability of the electrodeposited Bi film. At the time of writing, this experiment is on-going. After 10 weeks, there are no signs of mechanical failure and only a slight increase in transmission, which is likely due to the oxidation of metal in the presence of a strong oxidizer in perchloric acid (see Note S8, Supporting Information).
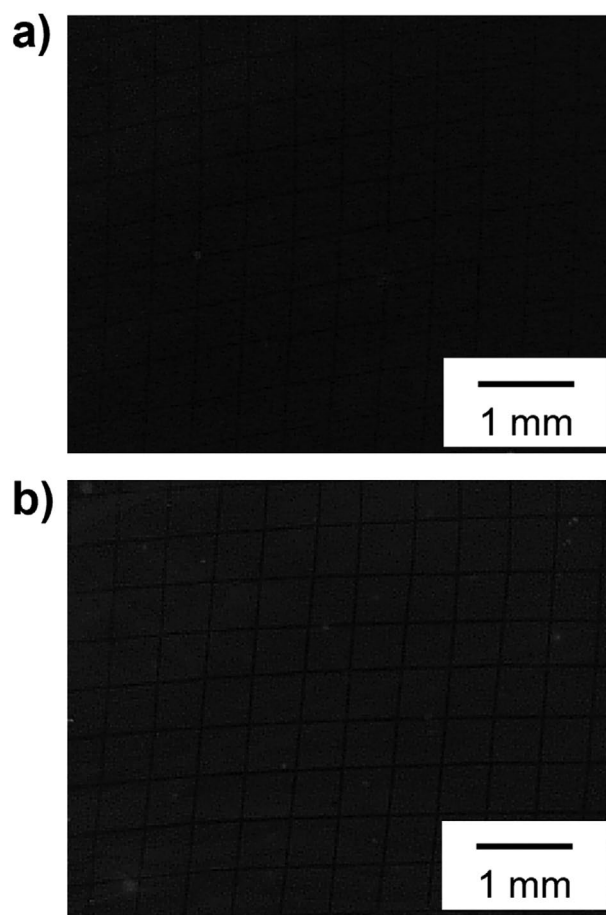

Figure 5. Microscope images of Bi-based device tinted to privacy state transmission a) immediately and b) 9 weeks after tinting and unplugging.

2202843 (5 of 8)

**ADVANCED
SCIENCE NEWS**
www.advancedsciencenews.com

**ADVANCED
ENERGY
MATERIALS**
www.advenergymat.de

3. Conclusion

In this work, we identified a serious mechanical reliability problem in Cu–Bi films tinted to 0.1% transmission where films crack and delaminate in <24 h. The presence of tensile stress combined with the corrosive nature of the electrolyte resulted in the failure in Cu–Bi. We showed that Cu and Bi single metal systems behave differently, with Cu films having tensile stress and Bi ones having compressive stress. Cu^{2+} from $Cu(ClO_4)_2$ causes mechanical failure in Cu-containing films. These failures are consistent with stress corrosion cracking and resemble characteristics of the surface mobility mechanism. This catastrophic failure due to SCC is pervasive and makes the window unsuitable for fenestration application. Bi, on the other hand, deposits under compression and is not susceptible to SCC, resulting in superior mechanical stability with no mechanical failure for more than 9 weeks in a device. This study demonstrates the importance of characterizing stress in electrodeposited films to identify susceptibility to mechanical failure driven by SCC. By doing so a framework of suitable metals for applications requiring electrodeposited metals to rest in their electrolyte can be designed. Metals such as Cd, In, Sn, Pb, and Bi are likely to have intrinsic resistance to SCC due to their lower melting point.[53] Despite their predicted stability Cd and Pb are likely to be avoided in fenestration application due to toxicity. Electrolytes tend to be less corrosive if they have salts with higher melting points.[66] Metals used for applications such as thermal camouflage and batteries (e.g., Ag, Zn, and Li) should have intrinsic susceptibility to SCC, so it is crucial to quantify stress and carefully consider the corrosivity of the environment. This work shows the first detailed study of mechanical reliability of electrodeposited films for window applications, paramount for their use in practical situations.

4. Experimental Section

Pt-Modified TCO Working Electrode Preparation: ITO on glass substrates were purchased from Xinyan Technology Ltd with glass thickness of 0.7 mm or Delta Technologies with thickness of 0.2 mm for substrate curvature experiments, both with nominal sheet resistance of 10 Ω □⁻¹ and were used as transparent conducting oxides (TCO). The TCO substrates were cleaned by sonication in 10 v/v% Extran in DI water solution, DI water, acetone, and then in isopropyl alcohol for 15 min each. The substrates were then dried with N_2 and cleaned in a UV–ozone cleaner for 15 min. Next, the TCO substrates were placed in a 10 mM 3-mercaptopropionic acid in ethanol solution and placed on a shaker for 24 h. The TCO substrates were then rinsed with ethanol then water before being placed in a Pt-nanoparticle solution (Sigma Aldrich) diluted 1:19 with DI water and placed on a shaker for 24–72 h. The TCO substrates were then rinsed with DI water, dried with N_2, then annealed at 250 °C for 25 min before use.

Electrolyte Preparation: Chemicals were bought and used without purification. The standard Cu–Bi electrolyte consisted of 10 mM $Cu(ClO_4)_2 \cdot 6H_2O$ (ACROS Organics), 10 mM $BiOClO_4 \cdot H_2O$ (GFS Chemicals), 10 mM $HClO_4$ (Alfa Aesar), and 1 M $LiClO_4 \cdot 3H_2O$ (ACROS Organics) with 0.1 w/v% PVA (31 000–50 000 g mol⁻¹, 97% hydrolyzed, Aldrich). PVA was added last and stirred at 1200 rpm and 60–70 °C until dissolved. Electrolytes designated as "X-based" were formed from the same base electrolyte but had only X as the active metal (i.e., "Cu-based" contained 1 M $LiClO_4$, 10 mM $HClO_4$, 10 mM $Cu(ClO_4)_2$, and 0.1 w/v% PVA).

Metal Counter Electrode Preparation: Cu mesh (100 mesh Copper 0.0012″ Wire Dia) and SS mesh (50 Mesh T316 Stainless High Transparency 0.0012″ Wire Dia) were bought from TWP, Inc. The metal electrodes were sonicated in acetone then DI water for 10 min each, then dried in an oven at 120 °C. The Cu meshes were then ready for use. The SS mesh was electrocleaned at 48 °C at –7 V for 5 min using a SS rod as both a counter and reference electrode (Electro-Cleaner Solution, Gold Plating Services). The SS mesh was then rinsed with DI water before being submerged in the TriVal 24 K Acid Gold strike bath at room temperature at –7 V for 5 s using a Pt plated Ti rod as both a counter and reference electrode (TriVal Gold Strike, Gold Plating Services). The SS mesh was again rinsed with DI water then Bi was electroplated at –0.7 V versus Ag/AgCl using the Bi-based electrolyte and a Pt wire counter electrode to the desired capacity. The Bi-Au-SS mesh was then rinsed in DI water then dried at 120 °C for 2 h before use.

RME Dynamic Window Fabrication: Two-electrode devices used Pt-modified TCO on glass substrates (Pt-TCO) as a working electrode and a metal counter electrode. Two layers of butyl rubber edge seal (Quanex: Solargain edge tape LP03, 1.7 mm thickness) separated the two electrodes and encapsulated the electrolyte between the Pt-ITO and back piece of glass. Conductive tape (Conducty Z22, ElectricMosaic) was used to make electrical contact with the working electrode. Edges were sealed at 110–120 °C with a weight, then the fully sealed devices were injected with electrolyte, and then sealed with a soldering iron.

Electrochemical Characterization: Electrochemical experiments were run using a BioLogic SP-150 potentiostat. Three-electrode experiments used a Pt wire counter electrode and a "no-leak" Ag/AgCl (eDAQ) reference electrode and tinting was performed at –0.7 V versus Ag/AgCl. Two-electrode devices were tinted at –0.7 V versus the counter electrode (Cu mesh or Bi–Au–SS mesh).

Soaking Tests: Soaking tests were performed in an oxygen free environment to eliminate the oxidation of metal in the presence of H^+ and O_2. Films were plated on the benchtop before being moved into an N_2 MBRAUN wetbox for soaking. Soaking electrolytes were sparged with N_2 for at least 30 min before bringing into the wetbox. Devices were injected and sealed inside the wetbox before removing to the benchtop for testing. See Note S1, Supporting Information, for more details.

Characterization: Ocean Optics OCEAN FX Miniature spectrometer was used in a standard configuration with an Ocean Optics halogen light source (HL-2000) for transmission and reflection measurements. Microscope images were taken with DinoLite USB microscope (AM3111) and an Amazon Basics Portable Photo Studio and Artograph PRO1200 LightPad. SEM-EDS was run using a FEI Nova 600i HITACHI SU3500 scanning electron microscope operated at an accelerating voltage of 5 kV and equipped with an EDS detector. A Rigaku DMAX XRD with Cu rotating anode was used in Bragg–Brantano geometry to generate θ–2θ diffraction patterns. For XRD:$Sin^2\Psi$ measurements the parallel beam geometry was used. Height alignment was performed for all samples to avoid peak shifts due to subtle differences in sample heights/thicknesses. See Note S5, Supporting Information, for more details. Substrate curvature and film thickness measurements were run using a DektakXT Stylus Profiler with a 2 µm stylus. See Note S2, Supporting Information, for more details.

Supporting Information

Supporting Information is available from the Wiley Online Library or from the author.

Acknowledgements

Conflict of Interest

M.D.M. is a co-founder of Tynt Technologies, a company commercializing reversible metal electrodeposition dynamic windows. All the other authors declare no conflict of interest.

Author Contributions

G.R.M. and A.L.Y. contributed equally to this work. G.R.M contributed to the writing the original draft, writing the review and editing, validation, conceptualization, investigation, and methodology. A.L.Y. contributed to the writing of the original draft, writing the review and editing, validation, conceptualization, investigation, and methodology. Y.C. contributed to the investigation, validation, methodology, and writing the review and editing. C.J.B. contributed to the writing the review and editing, funding acquisition, and supervision. M.D.M. contributed to the writing the review and editing, funding acquisition, supervision, and project administration.

Data Availability Statement

Research data are not shared.

Keywords

dynamic windows, mechanical stability, reversible metal electrodeposition, stress corrosion cracking

[1] Q. Wang, B. Liu, Y. Shen, J. Wu, Z. Zhao, C. Zhong, W. Hu, *Adv. Sci.* **2021**, *8*, 2101111.

[2] J. Liu, Z. Bao, Y. Cui, E. J. Dufek, J. B. Goodenough, P. Khalifah, Q. Li, B. Y. Liaw, P. Liu, A. Manthiram, Y. S. Meng, V. R. Subramanian, M. F. Toney, V. V. Viswanathan, M. S. Whittingham, J. Xiao, W. Xu, J. Yang, X.-Q. Yang, J.-G. Zhang, *Nat. Energy* **2019**, *4*, 180.

[3] Y. Qi, C. Ban, S. J. Harris, *Joule* **2020**, *4*, 2599.

[4] F. Wang, O. Borodin, T. Gao, X. Fan, W. Sun, F. Han, A. Faraone, J. A. Dura, K. Xu, C. Wang, *Nat. Mater.* **2018**, *17*, 543.

[5] X. Tao, D. Liu, T. Liu, Z. Meng, J. Yu, H. Cheng, *Adv. Funct. Mater.* **2022**, *32*, 2202661.

[6] S. Araki, K. Nakamura, K. Kobayashi, A. Tsuboi, N. Kobayashi, *Adv. Mater.* **2012**, *24*, OP122.

[7] G. Cai, P. Darmawan, X. Cheng, P. S. Lee, *Adv. Energy Mater.* **2017**, *7*, 1602598.

[8] X.-H. Li, C. Liu, S.-P. Feng, N. X. Fang, *Joule* **2019**, *3*, 290.

[9] K.-H. Chen, K. N. Wood, E. Kazyak, W. S. LePage, A. L. Davis, A. J. Sanchez, N. P. Dasgupta, *J. Mater. Chem. A* **2017**, *5*, 11671.

[10] K. N. Wood, M. Noked, N. P. Dasgupta, *ACS Energy Lett.* **2017**, *2*, 664.

[11] M. Krarti, *J. Build. Eng.* **2022**, *45*, 103462.

[12] A. Hedge, *Ergonomics Int. J.* **2018**, *2*, 000166.

[13] A. Hedge, D. Nou, *Proc. Hum. Factors Ergon. Soc. Annu. Meet.* **2018**, *62*, 378.

[14] C. J. Barile, D. J. Slotcavage, J. Hou, M. T. Strand, T. S. Hernandez, M. D. McGehee, *Joule* **2017**, *1*, 133.

[15] T. S. Hernandez, C. J. Barile, M. T. Strand, T. E. Dayrit, D. J. Slotcavage, M. D. McGehee, *ACS Energy Lett.* **2018**, *3*, 104.

[16] M. T. Strand, C. J. Barile, T. S. Hernandez, T. E. Dayrit, L. Bertoluzzi, D. J. Slotcavage, M. D. McGehee, *ACS Energy Lett.* **2018**, *3*, 2823.

[17] S. M. Islam, T. S. Hernandez, M. D. McGehee, C. J. Barile, *Nat. Energy* **2019**, *4*, 223.

[18] T. S. Hernandez, M. Alshurafa, M. T. Strand, A. L. Yeang, M. G. Danner, C. J. Barile, M. D. McGehee, *Joule* **2020**, *4*, 1501.

[19] M. T. Strand, T. S. Hernandez, M. G. Danner, A. L. Yeang, N. Jarvey, C. J. Barile, M. D. McGehee, *Nat. Energy* **2021**, *6*, 546.

[20] C. G. Granqvist, M. A. Arvizu, İ. Bayrak Pehlivan, H.-Y. Qu, R.-T. Wen, G. A. Niklasson, *Electrochim. Acta* **2018**, *259*, 1170.

[21] V. K. Thakur, G. Ding, J. Ma, P. S. Lee, X. Lu, *Adv. Mater.* **2012**, *24*, 4071.

[22] A. L. Yeang, T. S. Hernandez, M. T. Strand, D. J. Slotcavage, E. Abraham, I. I. Smalyukh, C. J. Barile, M. D. McGehee, *Adv. Energy Mater.* **2022**, *12*, 2200854.

[23] P. R. Lewis, K. Reynolds, C. Gagg, C. Gagg, *Forensic Materials Engineering: Case Studies*, CRC Press, Boca Raton, FL **2003**.

[24] V. Kain, in *Stress Corrosion Cracking*, (Eds: V. S. Raja, T. Shoji), Woodhead Publishing, Sawston, Cambridge **2011**, pp. 199–224.

[25] F. King, *The Potential for Stress Corrosion Cracking of Copper Containers in a Canadian Nuclear Fuel Waste Disposal Vault*, Atomic Energy of Canada Ltd., Canada **1996**.

[26] K. Sieradzki, R. C. Newman, *Philos. Mag. A* **1985**, *51*, 95.

[27] P. Cai, S. Yu, X. Xu, M. Chen, C. Sui, G.-X. Ye, *Appl. Surf. Sci.* **2009**, *255*, 8352.

[28] G. Kravchenko, *Graduate Thesis*, University of South Florida, Tampa, FL **2008**.

[29] A. Yuse, M. Sano, *Nature* **1993**, *362*, 329.

[30] M.-É. Schwaab, T. Biben, S. Santucci, A. Gravouil, L. Vanel, *Phys. Rev. Lett.* **2018**, *120*, 255501.

[31] O. Savchuk, A. A. Volinsky, *Measurement* **2021**, *177*, 109238.

[32] G. G. Stoney, C. A. Parsons, *Proc. R. Soc. Lond., Ser. A* **1909**, *82*, 172.

[33] E. Chason, A. Engwall, F. Pei, M. Lafouresse, U. Bertocci, G. Stafford, J. A. Murphy, C. Lenihan, D. N. Buckley, *J. Electrochem. Soc.* **2013**, *160*, D3285.

[34] W. D. Nix, B. M. Clemens, *J. Mater. Res.* **1999**, *14*, 3467.

[35] G. Abadias, E. Chason, J. Keckes, M. Sebastiani, G. B. Thompson, E. Barthel, G. L. Doll, C. E. Murray, C. H. Stoessel, L. Martinu, *J. Vac. Sci. Technol., A* **2018**, *36*, 020801.

[36] T. Pienkos, A. Proszynski, D. Chocyk, L. Gladyszewski, G. Gladyszewski, *Microelectron. Eng.* **2003**, *70*, 442.

[37] S. J. Hearne, J. A. Floro, *J. Appl. Phys.* **2005**, *97*, 014901.

[38] S. Armyanov, G. Sotirova-Chakarova, *J. Electrochem. Soc.* **1992**, *139*, 3454.

[39] T. D. Ziebell, C. A. Schuh, *J. Mater. Res.* **2012**, *27*, 1271.

[40] P. M. Alexander, R. W. Hoffman, *J. Vac. Sci. Technol.* **1976**, *13*, 96.

[41] S. H. Brongersma, E. Kerr, I. Vervoort, A. Saerens, K. Maex, *J. Mater. Res.* **2002**, *17*, 582.

[42] S. Armyanov, G. Sotirova, *Surf. Coat. Technol.* **1988**, *34*, 441.

[43] B. Eren, L. Marot, G. Günzburger, P.-O. Renault, T. Glatzel, R. Steiner, E. Meyer, *J. Phys. D: Appl. Phys.* **2013**, *47*, 025302.

[44] S. C. Seel, C. V. Thompson, S. J. Hearne, J. A. Floro, *J. Appl. Phys.* **2000**, *88*, 7079.

[45] J. A. Brinkmanf, *Acta Metall.* **1955**, *3*, 140.

[46] Q. Luo, A. H. Jones, *Surf. Coat. Technol.* **2010**, *205*, 1403.

[47] V. Hauk, in *Structural and Residual Stress Analysis by Nondestructive Methods*, (Ed: V. Hauk), Elsevier Science B.V, Amsterdam **1997**, pp. 17–65.

[48] A. Wyss, A. S. Sologubenko, N. Mishra, P. A. Gruber, R. Spolenak, *J. Mater. Sci.* **2017**, *52*, 6741.

[49] C. L. Azanza Ricardo, G. Degan, M. Bandini, P. Scardi, *Mater. Sci. Forum* **2010**, *638–642*, 2464.

[50] E. Chason, J. W. Shin, S. J. Hearne, L. B. Freund, *J. Appl. Phys.* **2012**, *111*, 083520.

[51] L. Lu, L. B. Wang, B. Z. Ding, K. Lu, *J. Mater. Res.* **2000**, *15*, 270.

[52] D. A. Jones, *Principles and Prevention of Corrosion*, 2nd ed., Prentice Hall, Hoboken, NJ **1996**.

[53] J. R. Galvele, *Corros. Sci.* **1987**, *27*, 1.

[54] C. M. Giordano, G. S. Duffó, J. R. Galvele, *Corros. Sci.* **1997**, *39*, 1915.

[55] K. Sieradzke, J. S. Kim, *Acta Metall. Mater.* **1992**, *40*, 625.

[56] R. K. Dinnappa, H. B. Rudresh, S. M. Mayanna, *Surf. Technol.* **1980**, *10*, 363.

[57] L. M. C. Pinto, E. Spohr, P. Quaino, E. Santos, W. Schmickler, *Angew. Chem., Int. Ed.* **2013**, *52*, 7883.

[58] T. Gloriant, *J. Non-Cryst. Solids* **2003**, *316*, 96.

[59] R. Schweinfest, A. T. Paxton, M. W. Finnis, *Nature* **2004**, *432*, 1008.

[60] Lehigh Preserve, Investigation of grain boundary segregation and embrittlement mechanisms of the Cu–Bi system by analytical electron microscopy. https://preserve.lib.lehigh.edu/islandora/object/preserve%3Abp-10370048 (accessed: July 2022).

[61] P. Waters, A. A. Volinsky, *Exp. Mech.* **2007**, *47*, 163.

[62] M. W. Moon, H. M. Jensen, J. W. Hutchinson, K. H. Oh, A. G. Evans, *J. Mech. Phys. Solids* **2002**, *50*, 2355.

[63] M. Doerner, W. D. Nix, *Crit. Rev. Solid State Mater. Sci.* **1988**, *14*, 225.

[64] D. Fan, F. Q. Zhu, I. X. Shao, P. C. Searson, R. C. Cammarata, *MRS Online Proc. Libr.* **2004**, *781*, 42.

[65] G. P. Tiwari, R. S. Mehrotra, *Defect Diffus. Forum* **2008**, *279*, 23.

[66] F. Delamare, G. E. Rhead, *Surf. Sci.* **1971**, *28*, 267.